JACS
JOURNAL OF THE AMERICAN CHEMICAL SOCIETY

Communication

pubs.acs.org/JACS

Bimetallic FeNi Concave Nanocubes and Nanocages

Nafiseh Moghimi,[†] Marwa Abdellah,[†] Joseph Palathinkal Thomas,[†] Mamata Mohapatra,[‡] and K. T. Leung*[,†]

[†]WATLab and Department of Chemistry, University of Waterloo, Waterloo, Ontario, Canada N2L3G1

[‡]Department of Hydro & Electro Metallurgy, Institute of Minerals and Materials Technology, Council of Scientific & Industrial Research, Bhubaneswar 751 013, Odisha, India

Supporting Information

ABSTRACT: Concave nanostructures are rare because of their thermodynamically unfavorable shapes. We prepared bimetallic FeNi concave nanocubes with high Miller index planes through controlled triggering of the different growth kinetics of Fe and Ni. Taking advantage of the higher activity of the high-index planes, we then fabricated monodispersed concave nanocages via a material-independent electroleaching process. With the high-index facets exposed, these concave nanocubes and nanocages are 10- and 100-fold more active, respectively, toward electrodetection of 4-aminophenol than cuboctahedrons, providing a label-free sensing approach for monitoring toxins in water and pharmaceutical wastes.

Shape-dependent physicochemical properties of nanostructured materials are widely explored for advanced applications. A variety of growth methods have been used to control the shape of nanostructures of mostly noble metals in order to enhance their catalytic activity.[1] These methods commonly produce nanostructures with convex shapes enclosed by low-index {100}, {110}, and {111} facets as a result of minimization of the surface energy.[1a,d] Because of their high surface energies, high-index facets usually grow faster than the other facets, leaving them out of the exposed faces of the final shape during crystal growth.[2] Furthermore, the high densities of atomic steps, ledges, kinks, and dangling bonds present in these high-index facets lead to their high activity. As the exposed crystalline faces of a nanomaterial have a strong influence on both its reactivity and selectivity, it is desirable to have high-index facets. To date, only a few methods for producing nanostructures with high-index surfaces have been reported, and they can be categorized into two common approaches. One approach involves the use of external agents such as surfactants, reducing agents, or stabilizers to enforce the preferred growth orientations.[2a,3] However, these external agents may cover the pristine surfaces of the nanostructures, which invariably reduces the surface activity; this is often due to incomplete removal during postprocessing. The other approach involves carving concave nanostructures by removing material from as-prepared convex nanoparticles (NPs) by various procedures, including electrochemical pulses[2b,4] and galvanic replacement reactions.[5] However, these methods suffer from the need for multiple steps in the synthesis, as the NPs must be prepared beforehand as the starting materials.

As cuboid nanostructures are enclosed by {100} and {110} facets, concave cubes with their high index planes are generally rare. For non-noble metals, it has not been possible to make concave nanostructures with previous methods because of their inherently high reactivity. In a recent study, we showed that the morphology of the nanostructures of a bimetallic system obtained by an electrochemical method strongly depends on the ratio of starting materials.[6] In the present work, we found that it is possible to produce concave FeNi nanocubes using a one-step, surfactant-free electrochemical method by manipulating the growth kinetics of a bimetallic system. The advantage of highly reactive facets was explored further by developing nanocages with preferential etching at the center of the concave cubes through an electroleaching process, thereby introducing a new approach for synthesizing concave nanocages. The electrocatalytic activities of the concave nanocubes and nanocages were also evaluated by electro-oxidation of 4-aminophenol (4-AP) as a model chemical sensing reaction. It should be noted that 4-AP is an important organic compound that can be used for *Escherichia coli* (*E. coli*) detection and as an intermediate or degradation product in the synthesis of paracetamol in the pharmaceutical industry. While Fe and Fe-based bimetallic nanoparticles have been widely studied and used for remediation of groundwater contamination involving chlorinated and nitroaromatic organic compounds[7] and toxic metal ions (As, Cd, Cr, Pb),[8] no report on the use of these NPs to sense toxic contamination in the water is available. The present work therefore not only introduces two novel synthesis methods for producing these concave nanostructures but also offers new active nanomaterials for label-free sensing to monitor toxins in water and pharmaceutical wastes.

Figure 1a–c shows typical scanning electron microscopy (SEM) images of nanocubes obtained from three electrolytes with different relative Ni compositions by amperometry at 25 °C [for experimental details, see the Supporting Information (SI)]. These FeNi concave nanocubes all exhibited narrow size distributions with average sizes of 59, 63, and 80 nm for Ni contents of 22, 31, and 47%, respectively. Increasing the Ni content to 47% appeared to increase the concavity of the nanocubes (Figure 1c). For electrolytes with >50% Ni, the NPs became truncated spheres. A detailed discussion of the shape evolution of FeNi nanoparticles obtained in electrolytes with different Ni contents is given elsewhere.[6]

Received: June 2, 2013
Published: July 9, 2013

dx.doi.org/10.1021/ja405504q | J. Am. Chem. Soc. 2013, 135, 10958–10961

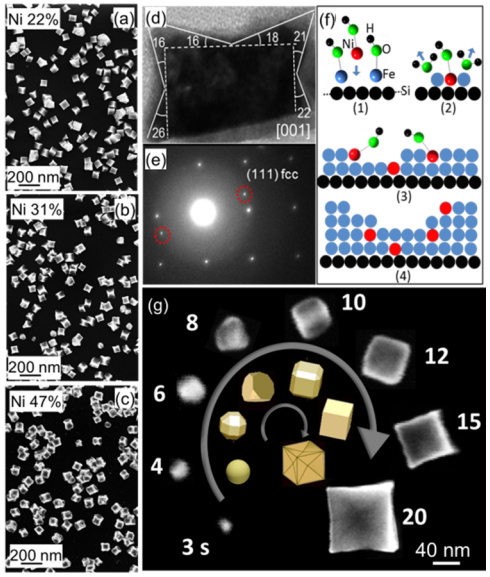

Figure 1. (a–c) SEM images of concave nanocubes with different Ni contents: (a) 22%; (b) 31%; (c) 47%. (d) HRTEM image of a concave FeNi nanocube with 47% Ni content and (e) the corresponding electron diffraction pattern projected from the [001] axis, with red circles marking the fcc spots in a bcc pattern. (f) Schematic diagram illustrating a plausible mechanism for the formation of higher-index facets of a concave nanocube: (1) selective adsorption of $FeOH^+$ over $NiOH^+$; (2) faster reduction of $FeOH^+$ than $NiOH^+$; (3, 4) formation of step or kink defects and ultimately higher-index planes. (g) SEM images of typical nanocubes (47% Ni) with increasing deposition time from 3 to 20 s.

To characterize the concavity of the FeNi nanocubes, we indexed the surface facets by cross-sectional transmission electron microscopy (TEM). Using a focused ion beam (FIB) to cut a 50 nm thick lamella of a typical FeNi concave NP (with 47% Ni content) on a Si substrate, we obtained a high-resolution TEM (HRTEM) image of the cross section of a single concave cube along the [001] direction (Figure 1d) and the corresponding electron diffraction pattern (Figure 1e). The observed diffraction pattern corresponds to the bcc FeNi pattern overlapping with the FeNi fcc pattern (spots marked by red circles), which shows that these NPs are in the mixed-phase region of the FeNi phase diagram.[6] Measuring the angles of the surface planes for the concave cube and a perfect cube and comparing them with those of an ideal concave cube (Figure S1 in the SI) showed that the surface of the concave nanocube is mainly enclosed by {720} facets along with some other high-index facets such as {520}, {730}, and {310}.

Thermodynamically, high-index facets, with their higher surface energies, are expected to grow faster than low-index facets, which generally results in their disappearance during crystal growth. The present formation of concave nanocubes with exposed high-index facets is therefore a kinetically driven process. Since pristine Fe NPs obtained under similar electrochemical deposition conditions have a well-defined cubic shape (Figure S2), the concavity of the FeNi nanocubes is caused by the presence of Ni. To investigate how Ni changes the shape of the Fe NPs from cubic to concave cubic in the absence of any surfactants or capping agents, we examined the role of kinetics in the formation mechanism in the present method. Electrochemical reduction of the Fe-group metal ions (M^{2+}) starts with the formation of MOH^+ ions in solution,[9] which are adsorbed onto the substrate surface and then reduced to the metal:[10]

$$MOH^+(aq) \xrightarrow{k_1} MOH^+(ads) \quad (1)$$

$$MOH^+(ads) + H^+ + 2e^- \xrightarrow{k_2} M + H_2O \quad (2)$$

Following the law of mass action, the adsorption rate depends on the concentration of M^{2+} and the number of free adsorption sites with rate constant k_1, while the reduction rate depends on the surface coverage of MOH^+ with rate constant k_2.[10] The early electroplating work on FeNi bulk alloy films showed higher adsorption and reduction rates for $FeOH^+$ than for $NiOH^+$.[10] Thus, in the present case the adsorbed $NiOH^+$ ions are most likely surrounded by adsorbed $FeOH^+$ ions in the first adlayer when reaction 1 occurs. This is followed by reduction of $FeOH^+$ to Fe (reaction 2), which occurs first at the $FeOH^+$-rich perimeter of the adlayer. The slower reduction of the adsorbed $NiOH^+$ inside the adlayer perimeter disrupts the growth of the (100) plane, creating step or kink defects. The next incoming ions (i.e., $FeOH^+$ or $NiOH^+$) therefore adsorb preferentially onto the defect sites, forming higher-index planes (Figure 1f). The presence of Cl^- and Ni^{2+} ions increases the rate of reduction of Fe ions, leading to kinetically favored (as opposed to thermodynamically favored) growth of NPs with higher-index facets. This was also observed in the formation of concave Au nanocubes when the rate of reduction of Au ions was enhanced by increasing the ascorbic acid concentration.[11]

To investigate the conditions under which kinetics becomes dominant over thermodynamics, we performed electrodeposition of FeNi NPs from an electrolyte containing 5 mM $NiCl_2$ and 5 mM $FeCl_2$ using deposition times of 3–20 s (Figure 1g and Figure S3). The FeNi NPs undergo significant morphological changes, from sphere to truncated cube to cube and finally to concave cube, with increasing deposition time. Since the shape of a NP is obtained by minimizing the energy of formation, a NP embryo must initially exist as a sphere because the surface area/volume ratio of a sphere (with the smallest critical radius, r^*) is the smallest.[12] Depending on the crystalline nature of the metal, nonspherical shapes can develop as a result of different surface energies of the exposed crystalline planes. For a NP of a particular shape, r^* is inversely proportional to the square of the shape factor (ξ):[12b]

$$r^* = 2\gamma/\Delta G_v \xi^2$$

where γ is the surface energy and ΔG_v is the volumetric free energy. As a result, each shape requires a specific minimal size to become thermodynamically stable. As the sphere ($\xi = 1$) continues to grow, the next stable shapes are truncated cube ($\xi = 0.922$) and cube ($\xi = 0.898$), because the surface energies for the exposed corners are generally greater than those of the edges, which are in turn greater than those of the surface planes. In accord with our observations, only after the cubic shape has been stabilized upon reaching the minimal size of 45–50 nm would the aforementioned kinetically driven mechanism become apparent. This kinetic effect therefore leads to stabilization of the thermodynamically unfavorable concave cubic shape.

With the presence of high-index facets, concave nanocubes should have higher chemical activities than NPs with low-index facets such as cuboctahedrons. To demonstrate the superior reactivity of these FeNi concave nanocubes, we synthesized FeNi cuboctahedrons with similar Ni content and size but convex surfaces, and we compared their electrochemical properties with those of the concave nanocubes. Figure 2a shows a SEM image of convex FeNi cuboctahedrons obtained by amperometry at 4 °C,

dx.doi.org/10.1021/ja405504q | J. Am. Chem. Soc. 2013, 135, 10958–10961

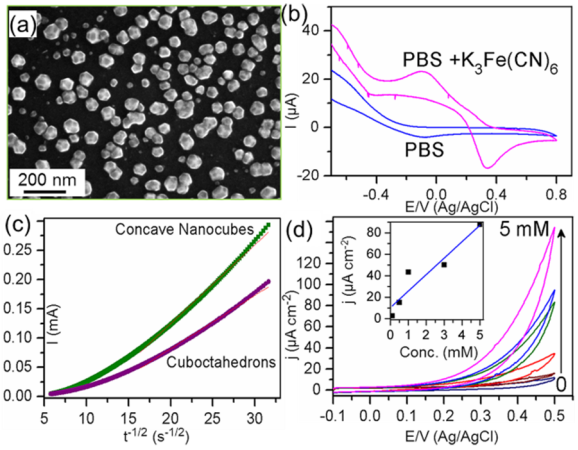

Figure 2. (a) SEM images of cuboctahedrons electrodeposited at 4 °C. (b) CVs of concave FeNi nanocubes in 10 mM PBS with and without 1 mM $K_3Fe(CN)_6$. (c) Cottrell plots obtained by chronoamperometery using FeNi concave nanocubes and cuboctahedrons as the working electrodes. (d) CVs of concave nanocubes at different concentrations of 4-aminophenol (scan rate = 50 mV s^{-1}). The inset shows the linear relationship between current density and concentration.

having a similar average size (75 nm) as the concave nanocubes in Figure 1c. The Ni content (as determined by energy-dispersive X-ray analysis) of the former (49%) was also similar to that of the latter (47%). Using FeNi concave nanocubes and convex cuboctahedrons deposited on Si substrates as the working electrodes in three-electrode cells (with a Pt wire and Ag/AgCl as the counter and reference electrodes, respectively), we performed chronoamperometry in 10 mM phosphate-buffered saline (PBS) containing 1 mM $K_3Fe(CN)_6$ at pH 7 to determine the electroactive surface areas for the two samples. From the cyclic voltammograms (CVs) of concave FeNi nanocubes in PBS with and without $K_3Fe(CN)_6$ (Figure 2b), the cyanide oxidation peak was found to be located at 370 mV vs Ag/AgCl. Therefore, for our chronoamperometric measurements we selected a step potential of 600 mV vs Ag/AgCl to be sufficiently higher than the oxidation peak of cyanide. The CVs of the cuboctahedrons were similar to those of concave nanocubes. From the resulting current−time (I−t) data, the electroactive areas (A) were obtained from the slopes of the I versus $t^{-1/2}$ plots shown in Figure 2c using the Cottrell equation:

$$I = nFAC_0D^{1/2}\pi^{-1/2}t^{-1/2}$$

where n is the number of electrons participating in the oxidation or reduction, F is the Faraday constant, D is the diffusion coefficient, and C_0 is the initial concentration of $K_3Fe(CN)_6$. The mass-normalized A value for the concave nanocube electrode was 6.7 m^2 g^{-1}, which is >3 times that of cuboctahedron electrode (2.1 m^2 g^{-1}), demonstrating the significantly higher reactivity of concave nanocubes relative to convex ones.

The high reactivity of these FeNi concave nanocubes opens up new opportunities for sensing biotoxins (e.g., *E. coli*) for water remediation and for monitoring of syntheses of drugs (e.g., paracetamol) in the pharmaceutical industry by electrochemical detection of 4-aminophenol (4-AP). 4-AP is an important "indicator molecule" because it is produced by hydrolysis of 4-aminophenyl-β-D-galactopyranoside by the enzyme β-galactosidase of *E. coli*[13] and is an intermediate or degradation product in drug synthesis.[14] Figure 2d shows CVs of concave FeNi nanocubes (with 47% Ni content) in a 10 mM PBS solution (pH 7) in the presence of different concentrations of 4-AP. No change in the shape of the concave nanocubes was observed after 20 cycles (Figure S4). Evidently, increasing the 4-AP concentration from 0.1 to 5 mM led to a higher oxidation current, as a linear relation between the current density (arbitrarily measured at 0.45 V vs Ag/AgCl) and the 4-AP concentration was obtained (Figure 2d inset). (The potential of 0.45 V was chosen because it is sufficiently high and close to the oxidation peak potential; the choice of this potential did not affect the relative performance among the NPs considered here.) Furthermore, the oxidation current obtained for the concave FeNi nanocubes at 0.45 V vs Ag/AgCl with 5 mM 4-AP was 10 times greater than that for the FeNi cuboctahedrons (Figure S5), again confirming the higher reactivity of the concave nanocubes. Among the other 4-AP sensing studies using HPLC or spectrophotometry, electrochemical detection has attracted a lot of recent attention because of its fast response and high sensitivity. Our result therefore shows excellent performance by the FeNi concave nanocubes, with a 4-AP detection sensitivity of 153 μA cm^{-2} mM^{-1}, which compares well with those of other detection systems (e.g., 33 and 177 μA cm^{-2} mM^{-1} for graphene−chitosan and graphene−polyaniline composites, respectively).[14]

To further increase the concavity of the nanocubes systematically, we introduce a controlled electroleaching process by applying cyclic voltammetry from −0.1 to 0.5 V vs Ag/AgCl in 10 mM PBS solution at pH 3. By controlling the number of CV scans, we could increase the concavity and eventually hollow out the interior of the nanocubes, producing concave nanocages. Figure 3a−c shows SEM images of the concave nanocages

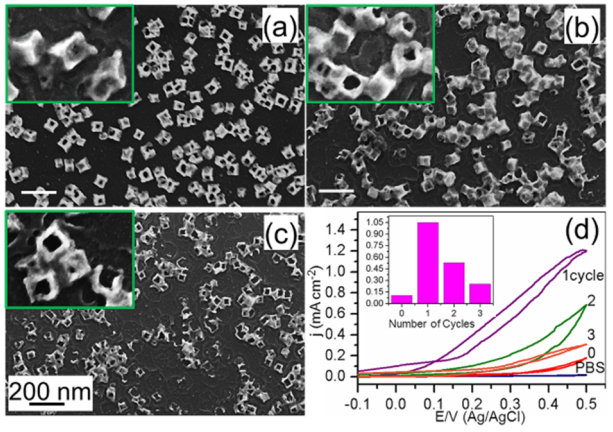

Figure 3. (a−c) SEM images of FeNi nanocages obtained after one, two, and three CV cycles in a 10 mM PBS solution at pH 3 and a scan rate of 50 mV s^{-1}. (d) CVs of concave nanocubes (with zero etching cycles) and the aforementioned concave nanocages in 5 mM 4-aminophenol in PBS (pH 7). The inset shows the corresponding current densities measured at 0.45 V vs Ag/AgCl for concave nanocubes after different numbers of CV cycles.

obtained after one, two, and three CV cycles. Material dissolution started at the center of the concave face, as expected because it has the highest strain and therefore the highest chemical potential.[15] Leaching continued to the edges until the center of the NP was completely hollowed out. In contrast, electroleaching of the cuboctahedrons resulted in the removal of the exterior surfaces, producing smaller cuboctahedrons with no sign of cage formation (Figure S6). It should be noted that metallic nanocages have traditionally been prepared by deposition of a

dx.doi.org/10.1021/ja405504q | J. Am. Chem. Soc. 2013, 135, 10958−10961

thin metal shell on polymer or silica beads followed by removal of the beads by calcination or wet-chemical etching[16] or by galvanic replacement reactions between Ag nanostructures and compounds of less reactive metals such as Au, Pt, and Pd.[17] The present synthesis of nanocages is therefore simple and does not have previously reported problems, including difficulty in removing the colloidal templates, poorly defined composition,[18] and unwanted coupling in dealloying.[19] We also performed the aforementioned reactivity test on these concave nanocages by measuring the oxidation current of 5 mM 4-AP in PBS at pH 7 as a function of the number of etching cycles. Remarkably, the concave nanocages obtained after the first CV cycle exhibited >10-fold enhancement in the current density measured at 0.45 V relative to concave nanocubes and >100-fold enhancement relative to the cuboctahedrons.

Even after the second and third cycles, this enhancement of the current density for the concave nanocages remained significant (i.e., 5 and 2.4 times that for concave nanocubes, respectively; Figure 3d inset). The remarkable enhancement found for the concave nanocages is due to the addition of high (and higher) index planes in the cavities of the nanocages and the higher active surface area. The reduction in the enhancement with repeated CV cycles is likely caused by desolation of higher-index planes and reductions in the active surface area. The sensitivity and limit of detection for the nanocages after the first CV cycle were 376 μA mM^{-1} cm^{-2} and 0.3 μM, respectively, confirming their high detection sensitivity relative to other sensors.[14,20]

Concave FeNi nanocubes and nanocages with high-index facets have been obtained by manipulating the kinetics of NP growth using a bimetallic system and by an electroleaching process, respectively. They exhibit remarkably high electroactivities (with >10- and >100-fold enhancement, respectively) for the detection of 4-aminophenol relative to FeNi cuboctahedrons with convex surfaces, making them one of the most electroactive nanostructures reported to date. We have also demonstrated for the first time that the present electroleaching method is a novel approach to the synthesis of cagelike nanostructures. The concave FeNi nanocages, with their hollow interiors and tunable cavity size, can be used not only as an exceptional sensor in a mild environment close to neutral pH but also for encapsulation and chemical trapping. Since the etching is driven by the high activity of the high-index planes located at the cavity, the present method of producing nanocages is material-independent and can be extended to any concave nanostructure.

■ ASSOCIATED CONTENT

Supporting Information

Experimental details, SEM images, and CVs. This material is available free of charge via the Internet at http://pubs.acs.org.

■ AUTHOR INFORMATION

Corresponding Author

tong@uwaterloo.ca

Notes

The authors declare no competing financial interest.

■ ACKNOWLEDGMENTS

This work was supported by the Natural Sciences and Engineering Research Council of Canada. N.M. thanks the Waterloo Institute for Nanotechnology for the WIN Fellowship. M.M. gratefully acknowledges the receipt of the BOYSCAST Fellowship supported by the Government of India.

■ REFERENCES

(1) (a) Xia, Y.; Xiong, Y.; Lim, B.; Skrabalak, S. E. *Angew. Chem., Int. Ed.* **2009**, *48*, 60. (b) Tao, A. R.; Habas, S.; Yang, P. *Small* **2008**, *4*, 310. (c) Wang, C.; Daimon, H.; Onodera, T.; Koda, T.; Sun, S. *Angew. Chem., Int. Ed.* **2008**, *47*, 3588. (d) Sun, Y.; Xia, Y. *Science* **2002**, *298*, 2176. (e) Zhang, J.; Li, S.; Wu, J.; Schatz, G. C.; Mirkin, C. A. *Angew. Chem., Int. Ed.* **2009**, *48*, 7787. (f) Jin, R.; Cao, Y. C.; Hao, E.; Me, G. S.; Schatz, G. C.; Mirkin, C. A. *Nature* **2003**, *425*, 487.

(2) (a) Ming, T.; Feng, W.; Tang, Q.; Wang, F.; Sun, L.; Wang, J.; Yan, C. *J. Am. Chem. Soc.* **2009**, *131*, 16350. (b) Tian, N.; Zhou, Z. Y.; Sun, S. G.; Ding, Y.; Wang, Z. L. *Science* **2007**, *316*, 732.

(3) (a) Lu, C. L.; Prasad, K. S.; Wu, H. L.; Ho, J. A.; Huang, M. H. *J. Am. Chem. Soc.* **2010**, *132*, 14546. (b) Huang, X.; Tang, S.; Zhang, H.; Zhou, Z.; Zheng, N. *J. Am. Chem. Soc.* **2009**, *131*, 13916. (c) Ma, Y.; Kuang, Q.; Jiang, Z.; Xie, Z.; Huang, R.; Zheng, L. *Angew. Chem., Int. Ed.* **2008**, *47*, 8901.

(4) Zhou, Z. Y.; Tian, N.; Huang, Z. Z.; Chen, D. J.; Sun, S. G. *Faraday Discuss.* **2008**, *140*, 81.

(5) Zhang, H.; Jin, M.; Wang, J.; Li, W.; Camargo, P. H. C.; Kim, M. J.; Yang, D.; Xie, Z.; Xia, Y. *J. Am. Chem. Soc.* **2011**, *133*, 6078.

(6) Moghimi, N.; Bazargan, S.; Pradhan, D.; Leung, K. T. *J. Phys. Chem. C* **2013**, *117*, 4852.

(7) (a) Song, H.; Carraway, E. R. *Environ. Sci. Technol.* **2005**, *39*, 6237. (b) Hong, Y.; Rheem, Y.; Lai, M.; Cwiertny, D. M.; Walker, S. L.; Myung, N. V. *Chem. Eng. J.* **2009**, *151*, 66.

(8) (a) Ponder, S. M.; Darab, J. G.; Mallouk, T. E. *Environ. Sci. Technol.* **2000**, *34*, 2564. (b) Kanel, S. R.; Manning, B.; Charlet, L.; Choi, H. *Environ. Sci. Technol.* **2005**, *39*, 1291.

(9) Vaes, J.; Fransaer, J.; Celis, J. P. *J. Electrochem. Soc.* **2000**, *147*, 3718.

(10) Matlosz, M. *J. Electrochem. Soc.* **1993**, *140*, 2272.

(11) Langille, M. R.; Personich, M. L.; Zhang, J.; Mirkin, C. A. *J. Am. Chem. Soc.* **2012**, *134*, 14542.

(12) (a) Vitos, L. *Surf. Sci.* **1998**, *411*, 186. (b) Huitink, D.; Kundu, S.; Park, C.; Mallick, B.; Huang, J. Z.; Liang, H. *J. Phys. Chem. A* **2010**, *114*, 5596.

(13) Pérez, F.; Tryland, I.; Mascini, M.; Fiksdal, L. *Anal. Chim. Acta* **2001**, *427*, 149.

(14) (a) Fan, Y.; Liu, J. H.; Yang, C. P.; Yu, M.; Liu, P. *Sens. Actuators, B* **2011**, *157*, 669. (b) Yin, H.; Ma, Q.; Zhou, Y.; Ai, S.; Zhu, L. *Electrochim. Acta* **2010**, *55*, 7102.

(15) Yang, W. H.; Srolovitz, D. J. *J. Mech. Phys. Solids* **1994**, *42*, 1551.

(16) (a) Oldenburg, S.; Averitt, R.; Westcott, S.; Halas, N. *Chem. Phys. Lett.* **1998**, *288*, 243. (b) Wang, Y.; Angelatos, A. S.; Caruso, F. *Chem. Mater.* **2008**, *20*, 848.

(17) (a) Selvakannan, P. R.; Sastry, M. *Chem. Commun.* **2005**, 1684. (b) Chen, J.; McLellan, J. M.; Siekkinen, A.; Xiong, Y.; Li, Z. Y.; Xia, Y. *J. Am. Chem. Soc.* **2006**, *128*, 14776.

(18) Kijima, T.; Yoshimura, T.; Uota, M.; Ikeda, T.; Fujikawa, D.; Mouri, S.; Uoyama, S. *Angew. Chem., Int. Ed.* **2004**, *43*, 228.

(19) Lu, X.; Au, L.; McLellan, J.; Li, Z. Y.; Marquez, M.; Xia, Y. *Nano Lett.* **2007**, *7*, 1764.

(20) Shiroma, L. Y.; Santhiago, M.; Gobbi, A. L.; Kubota, L. T. *Anal. Chim. Acta* **2012**, *725*, 44.